Am J Cancer Res 2026;16(8):3433-3444
www.ajcr.us /ISSN:2156-6976/ajcr0172292

Original Article

Aryl hydrocarbon receptor-dependent lipid droplet accumulation supports redox homeostasis in hypoxia-induced PCa cells

Yuan Yao, Shanshan Liang, Tianji He, Chenjun Ma, Guotong Gong, Xiang Chen, Jingsong Yu

Department of Urology, Liuzhou People's Hospital Affiliated to Guangxi Medical University, Liuzhou, Guangxi, The People's Republic of China

Received February 26, 2026; Accepted July 14, 2026; Epub August 15, 2026; Published August 30, 2026

Abstract: Tumor cells in hypoxic environments generate large amounts of reactive oxygen species (ROS), and lipid droplets (LDs) play an essential role in maintaining redox homeostasis under these harsh conditions. The aryl hydrocarbon receptor (AhR) is a member of the basic helix-loop-helix (bHLH) transcription factor superfamily that is closely associated with malignant tumor phenotypes. AhR has been shown to drive prostate cancer (PCa) cell growth, but the specific mechanistic basis for this effect remains unclear. In this study, we used a hypoxia-induced PC-3M cell model to explore the molecular pathways through which AhR promotes PCa progression. Significant LD accumulation was observed in hypoxia-induced PC-3M cells, and AhR knockdown inhibited LD formation, supporting a potential role for AhR in this process. AhR-dependent LD formation enhanced the ability of PC-3M cells to adapt to oxidative stress, as evidenced by reduced ROS production and a decreased NADP/NADPH ratio. AhR-dependent LD formation also alleviated mitochondrial dysfunction, as evidenced by increased membrane potential, reduced cell apoptosis, and decreased levels of active caspase-3. Treatment with the LD inhibitor PF-06424439 reversed these protective effects, as did DGAT2 knockdown. Mechanistically, AhR was found to activate the PI3K/AKT pathway through RAB3D, thereby promoting LD formation. Co-immunoprecipitation (Co-IP) experiments demonstrated that CYLD inhibits AhR activity by eliminating the K63-linked ubiquitination of AhR. In summary, under hypoxic conditions, these results indicate that AhR protects PCa cells from ROS-associated toxicity through the induction of LD formation.

Keywords: Prostate cancer, aryl hydrocarbon receptor, lipid drop, CYLD, ROS

Introduction

Prostate cancer (PCa) continues to pose a serious threat to male health throughout the globe, with the highest cumulative incidence among all male malignancies [1]. As PCa is a hormone-dependent cancer, androgen deprivation therapy has long been used as the first-line approach for its treatment [2]. Although significant progress has been made in diagnosing and treating PCa over the past decade, the incidence of PCa continues to rise due to various factors [3]. Conventional treatment methods can only facilitate disease control for a limited duration, and many patients will subsequently develop refractory androgen-independent PCa [4, 5]. At present, the mechanism by which PCa cells acquire the ability to grow and invade in the absence of hormone stimulation remains incompletely understood, underscoring the need for systematic analyses of PCa pathogenesis and the identification of novel therapeutic targets.

Tumor cells exhibit a remarkable ability to adapt to adverse environmental conditions. Solid tumor cell exposure to hypoxic microenvironments can trigger the generation of large quantities of reactive oxygen species (ROS) [6]. Prolonged exposure to high levels of ROS, in turn, may induce oxidative stress-dependent cell death [7]. Lipid droplets (LDs) are essential organelles for lipid storage, but LD accumulation in non-adipose cells is a recognized marker of carcinogenesis [8]. Notably, LDs can protect tumor cells from oxidative stress-induced damage in hypoxic microenvironments [9].

https://doi.org/10.62347/HYGZ1071

The aryl hydrocarbon receptor (AhR) is a member of the basic helix-loop-helix (bHLH) transcription factor superfamily [10]. AhR expression is upregulated in most tumor cells and is closely associated with tumor proliferation, invasion, metastasis, and immune evasion [11], with specific evidence for the ability of AhR to promote PCa cell proliferation [12]. AhR has also been reported to facilitate the accumulation of LDs in various cell types [13, 14]. In PCa, more LDs are detectable in cancerous tissues as compared to normal tissues [15]. Based on these observations, we hypothesized whether AhR influenced the progression of PCa through LDs.

CYLD lysine 63 deubiquitinase (CYLD), a member of the USP family, is a deubiquitinating enzyme that specifically removes K63-linked ubiquitin chains from target proteins [16]. AhR can undergo K63 ubiquitination that activates the AhR signaling pathway [17]. CYLD deficiency has also previously been shown to stimulate PCa cell proliferation and survival [18]. This suggests that lower levels of CYLD expression may, at least in part, maintain the K63 ubiquitination of AhR, thereby activating the AhR pathway and promoting PCa progression.

To test these hypotheses in the present study, we employed PC-3M cells, which are a human androgen receptor-negative and androgen-independent PCa cell line. By modulating AhR expression in hypoxia-induced PC-3M cells, we sought to delineate the molecular mechanism by which AhR promotes PCa progression.

Materials and methods

Cell culture and hypoxic treatment

The hormone-insensitive human PC-3M cell line (iCell Bioscience Inc., Shanghai, China) was cultured in RPMI-1640 medium (Solarbio Science & Technology, Co., Ltd., Beijing, China) supplemented with 10% fetal calf serum (Tianhang, Hangzhou, China). For experiments under hypoxic conditions, PC-3M cells were incubated in a hypoxic chamber maintained at 1% O_2 and 5% CO_2 at 37°C for 48 h.

Cell transfection and treatment

AhR or CYLD overexpression constructs (oe-AhR or oe-CYLD) and corresponding control (oe-NC) were cloned and inserted into the pcDNA3.1 vector. AhR interference sequences (sh-AhR#1, sh-AhR#2) and RAB3D interference sequence (shRAB3D) were synthesized and cloned into the pRNA-H1.1 vector. A scrambled shRNA served as the negative control. For transfection, cells were seeded into 6-well plates for 24 h. Transfection was performed using Lipofectamine 3000 (Invitrogen, Carlsbad, CA, USA). To inhibit LD formation, PC-3M cells were treated with 10 μM PF-06424439 (MedChemExpres, Shanghai, China) for 48 h. To suppress PI3K/AKT pathway activity, PC-3M cells were treated with 10 μM LY294002 (Macklin, Shanghai, China) for 48 h.

Oil red O staining

The culture medium of treated PC-3M cells was removed, and cells were washed twice in PBS. Next, cells were fixed with ORO solution for 20 min before staining. The cells were incubated in 60% isopropanol for 20 s, and then incubated in oil red O staining solution for 10 min. Finally, the cells were washed twice and photographed. Oil red O was then extracted with isopropanol for 10 min, and the absorbance of the extracted solution was detected at 490 nm.

RNA isolation and real-time PCR analysis

Total RNA from PC-3M cells was extracted using the TRIpure reagent (BioTeke Bio., Beijing, China). Reverse transcription was conducted with the All-in-One First-Strand SuperMix kit (Magen, Guangzhou, China) using 1 μg of RNA. Real-time quantitative PCR was performed with the SYBR Green mix (Solarbio Science & Technology, Co., Ltd., Beijing, China) on a real-time PCR system (aperbio, Suzhou, China). The thermocycler protocol consisted of an initial pre-denaturation step at 95°C for 5 min, followed by 40 cycles of 95°C for 10 s, 60°C for 10 s, and 72°C for 15 s. $2^{-\Delta\Delta Ct}$ method was used to quantify the related level of gene expression. Primers were as follows: AhR (forward, 5'-AAAAGAAAGGGAAAGATGG-3', reverse, 5'-TATGGGACTCGGCACAA-3'), RAB3D (forward, 5'-CTACCGCACCATCACCA-3', reverse, 5'-CCTCAGCAGGCACAACA-3'), CYLD (forward, 5'-TTGCAGAGGCACCATCATGT-3', reverse, 5'-GTCCGGATCGTCGTAGCATT-3'), and β-actin (forward, 5'-TTGCCGACAGGATGCAGAAGGA-3', reverse, 5'-AGGTGGACAGCGAGGCCAGGAT-3').

Western blotting (WB)

Equal amounts of protein were analyzed by SDS-PAGE and then transferred to the PVDF

membrane (Abcam, Cambridge, UK). Blots were then blocked for 1 h with blocking buffer (Beyotime Biotech Co., Ltd., Shanghai, China) at 37°C, followed by incubation with primary antibodies overnight at 4°C. Membranes were then washed with washing buffer (Beyotime Biotech Co., Ltd., Shanghai, China) three times and incubated at room temperuture for 60 min with diluted (1:5000) secondary HRP-labeled IgG (goat anti-mouse IgG, Cat. No. A0216, Beyotime Biotech Co., Ltd., Shanghai, China; goat anti-rabbit IgG, A0208, Beyotime Biotech Co., Ltd., Shanghai, China). The primary antibodies were as follows: AhR (1:1000, Thermo Fisher Scientific Inc., Cat. No. MA1-513, Pittsburgh, PA, USA), DGAT2 (1:1000, ABclonal Biotechnology Co., Ltd., Cat. No. A13891, Wuhan, China), p-PI3K (1:500, ABclonal Biotechnology Co., Ltd., Cat. No. AP0427), PI3K (1:500, ABclonal Biotechnology Co., Ltd., Cat. No. A4992), p-AKT (1:500, ABclonal Biotechnology Co., Ltd., Cat. No. AP0637), AKT (1:500, ABclonal Biotechnology Co., Ltd., Cat. No. A22412), RAB3D (1:500, ABclonal Biotechnology Co., Ltd., Cat. No. A10390), CYLD (1:500, proteintech, Cat. No. 11110-1-AP), Histone H3 (1:80000, ABclonal Biotechnology Co., Ltd., Cat. No. AC070), and β-actin (1:20000, 1:500, ABclonal Biotechnology Co., Ltd., Cat. No. AC038).

ROS analyses

ROS levels in PC-3M cells were measured using the fluorescent DCFH-DA probe (Biosharp Life Sciences, Hefei, China). Briefly, the treated-PC-3M cells were exposed to 10 μM DCFH-DA for 30 min in the dark. Then, cells were washed with serum-free cell culture medium and analyzed using a fluorescence microscope.

NADP+/NADPH quantificatio

PC-3M cell samples were prepared according to the manufacturer's instructions for the $NADP^+$/NADPH Quantification Kit (Biosharp Life Sciences, Hefei, China). Sample supernatants from PC-3M cells were collected and analyzed for $NADP^+$ and NADPH. $NADP^+$ and NADPH content were quantified at 450 nm using a microplate reader.

Caspase-3 activity assay

PC-3M cells were collected and lysed with the Caspase-3 Activity Detection Kit (Solarbio Science & Technology, Co., Ltd., Beijing, China) as directed. Protein concentrations were detected using the Bradford Protein Concentration Determination Kit (Biosharp Life Sciences, Hefei, China). Finally, the absorbance was measured using a plate reader at 405 nm, and the caspase-3 activity was calculated according to the absorbance.

JC-1 analysis

To evaluate mitochondrial membrane potential, PC-3M cells were collected and resuspended with culture medium, followed by incubation with JC-1 staining solution (Biosharp Life Sciences, Hefei, China) for 20 min at 37°C. Cells were then collected and washed twice with JC-1 staining buffer (Biosharp Life Sciences, Hefei, China). Finally, stained cells were analyzed by flow cytometry.

Apoptosis

Appropriately treated PC-3M cells were collected and stained with 5 μL of Annexin V-FITC and 10 μL PI (Biosharp Life Sciences, Hefei, China). Flow cytometric analysis was performed with a FACS Calibur instrument (Agilent, USA).

Co-Immunoprecipitation (Co-IP)

Whole-cell extracts from treated PC-3M cells were lysed on ice using a lysis solution containing 1 mM PMSF. Cell supernatants were centrifuged (10,000×g, 5 min) at 4°C, and the protein therein was quantified using a BCA kit (Beyotime Biotech Co., Ltd., Shanghai, China). Antibodies were immobilized on AminoLink coupling resin. Then, cell supernatants were separately added to the corresponding resins, and the samples were shaken gently for 2 h at room temperature. Subsequently, the target protein-antibody complex was eluted and analyzed by Western blotting. The following antibodies were used for Co-IP: anti-AhR (1:1000, Thermo Fisher Scientific Inc., Cat. No. MA1-513, Pittsburgh, PA, USA), anti-CYLD (1:500, Proteintech, 11110-1-AP, Wuhan, China), and anti-Ubi-k63 (1:1000, Abcam, Cat. No. ab179434, Cambridge, UK). Goat anti-mouse IgG (1:5000, Beyotime Biotech Co., Ltd., Cat. No. A0216, Shanghai, China) and goat anti-rabbit IgG (1:5000, Beyotime Biotech Co., Ltd., Cat. No. A0208, Shanghai, China).

Immunofluorescence (IF)

Each cell slide was fixed with 4% paraformaldehyde for 15 min and then gently washed three

times with PBS. The cells were then blocked with 0.1% TritonX-100 for 30 min and 1% BSA for 15 min. Next, cells were incubated with primary anti-AhR (1:100, Thermo Fisher Scientific Inc., Cat. No. MA1-513, Pittsburgh, PA, USA) overnight at 4°C, washed with PBS, and incubated with an Alexa Fluor® 488-conjugated secondary antibody (1:200, Cell Signaling Technology, Cat. No. 4408, Danvers, MA, USA) for 1 h at room temperature. Finally, the cells were counterstained with DAPI (Aladdin Regents Co., Ltd., Shanghai, China), mounted on glass slides, and imaged using a fluorescence microscope (Olympus, Japan).

Data analysis

All experiments were carried out in triplicate to ensure reproducibility, and all data were analyzed with GraphPad Prism 9. Normality was assessed prior to statistical analysis. For normally distributed data, two-group comparisons were performed using unpaired t-tests, while Welch's t-test was used when homogeneity of variance was not satisfied. One-way ANOVAs followed by Tukey's post hoc test were used for comparisons among three groups. Data are presented as mean ± standard deviation for all groups. $P < 0.05$ was considered significant.

Results

AhR promotes LD accumulation in hypoxia-induced PC-3M cells

As shown in **Figure 1A**, a significant increase in LD accumulation was evident in PC-3M cells under hypoxic conditions. Western blotting demonstrated that AhR was activated under hypoxic conditions, as evidenced by increased nuclear AhR expression (**Figure 1B**). To investigate the potential involvement of AhR in this process, AhR was overexpressed (**Figure 1C**) and knocked down in PC-3M cells (**Figure 1D**). Strikingly, AhR overexpression promoted LD formation in PC-3M cells under hypoxic conditions, while AhR knockdown inhibited the accumulation of LDs (**Figure 1E**). This indicates that AhR promotes the formation of LDs in PC-3M cells under hypoxic conditions.

AhR-dependent LD biogenesis promotes oxidative stress adaptation in PC-3M cells and alleviates mitochondrial dysfunction

A previous study has demonstrated the ability of AhR to promote PCa progression [12]. To test the potential involvement of LDs in this process, we examined the effects of hypoxia on PC-3M cells, and then performed loss-of-function experiments by either treating AhR-overexpressing PC-3M cells with the LD inhibitor PF-06424439 or knocking down DGAT2 (a key triglyceride synthesis enzyme that directly blocks LD formation) with an shRNA construct (**Figure 2A**). DGAT2 knockdown efficiency was confirmed by Western blotting (Supplementary Figure 1A). Hypoxia induced ROS production in PC-3M cells (**Figure 2B**), whereas AhR overexpression significantly decreased ROS levels (**Figure 2D**) and the NADP/NADPH ratio (**Figure 2C**), consistent with the alleviation of cellular oxidative damage. Notably, both PF-06424439 treatment and DGAT2 knockdown reversed these effects, leading to increased ROS production and elevated NADP/NADPH ratios (**Figure 2C**, **2D**; Supplementary Figure 1B, 1C). These findings indicate that the inhibition of ROS generation and the enhancement of cellular antioxidant capacity by AhR under hypoxic conditions are strictly dependent on LD formation.

Moreover, we assessed mitochondrial transmembrane potential and apoptotic signaling activity in PC-3M cells. AhR overexpression reduced the number of JC-1 monomers (**Figure 2E**), consistent with the alleviation of mitochondrial damage. Additionally, AhR overexpression inhibited apoptosis, as evidenced by a reduction in apoptotic cells (**Figure 2F**) and a decrease in active caspase-3 levels (**Figure 2G**). Importantly, the protective effects of AhR on mitochondrial function and apoptosis were effectively reversed following either PF-06424439 treatment or DGAT2 knockdown (**Figure 2E-G**; Supplementary Figure 1D-F). Collectively, these pharmacological inhibition and genetic knockdown results demonstrate that AhR alleviates mitochondrial dysfunction and apoptosis in PC-3M cells under hypoxic conditions by promoting the formation of LDs.

AhR promotes LD formation via PI3K/AKT pathway activation

Next, we investigated the mechanism by which AhR regulates the formation of LDs. Hypoxia induced an increase in the phosphorylation levels of PI3K (p-PI3K) and AKT (p-AKT) in cells, consistent with PI3K/AKT signaling pathway activation (Supplementary Figure 2A, 2B). p-PI3K and p-AKT levels were further elevated

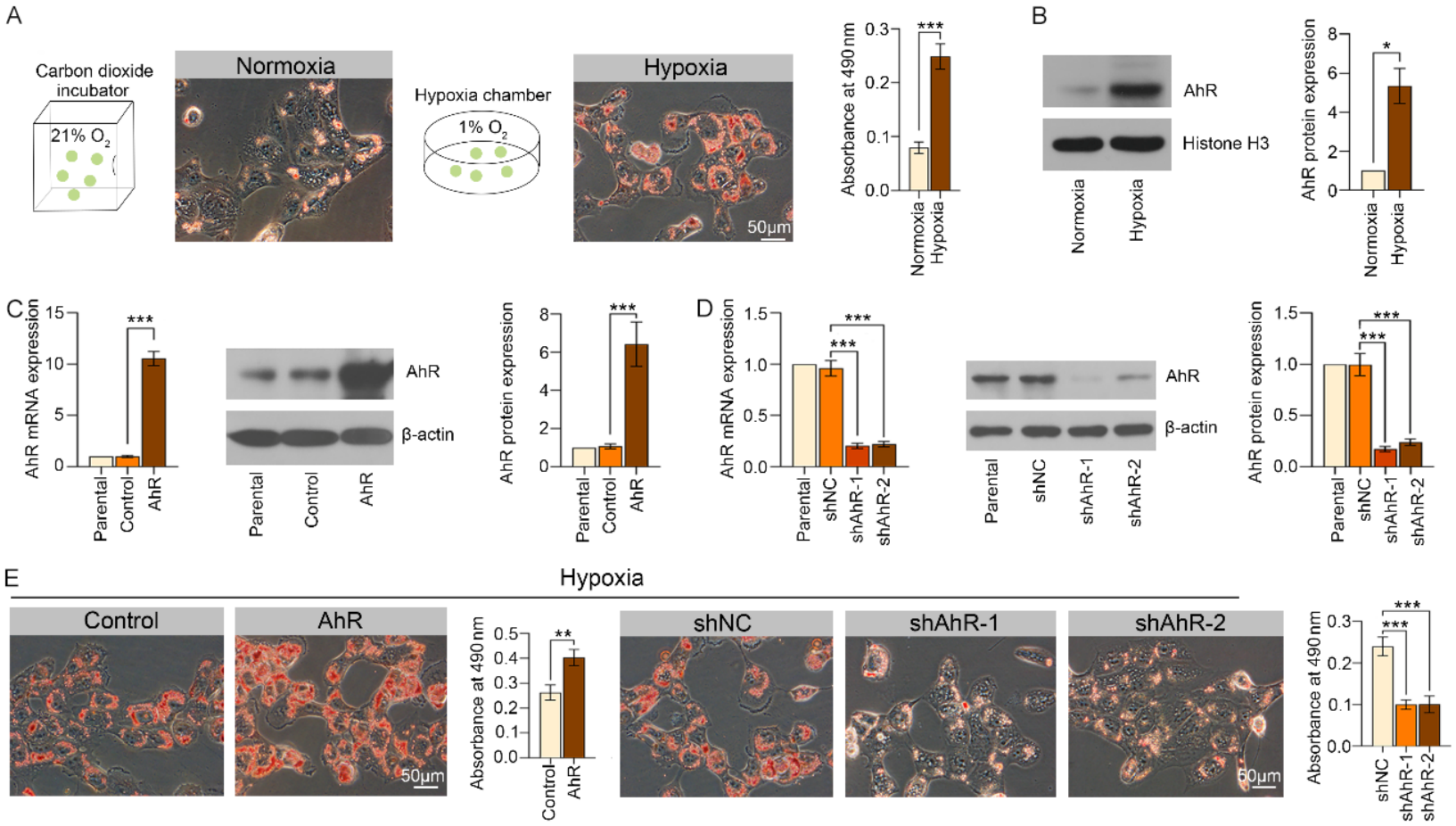

Figure 1. AhR promotes lipid droplet (LD) accumulation in hypoxia-induced PC-3M cells. (A) PC-3M cells were maintained under normoxic or hypoxic conditions for 48 h, and Oil red O staining was performed. Representative images of LDs in PC-3M cells were then captured with corresponding quantification. Student's t-test, ***P < 0.001, Hypoxia vs. Normoxia. n = 3, Scale bar, 50 μm, 400×. (B) Nuclear AhR expression was increased in hypoxia-induced PC-3M cells. *P < 0.05, Hypoxia vs. Normoxia. n = 3. (C, D) AhR was overexpressed (C) or knocked down (D) in PC-3M cells, after which AhR expression was analyzed by Real-time PCR and western blotting. One-way ANOVA, ***P < 0.001, AhR vs. Control, shAhR-1/shAhR-2 vs. shNC. n = 3. (E) Oil red O staining was used to detect the effect of AhR overexpression or knockdown on LD formation in PC-3M cells under hypoxic conditions. Scale bar, 50 μm, 400×. Student's t-test, **P < 0.01, AhR vs. Control; One-way ANOVA, ***P < 0.001, shAhR-1/shAhR-2 vs. shNC. n = 3, Scale bar, 50 μm, 400×.

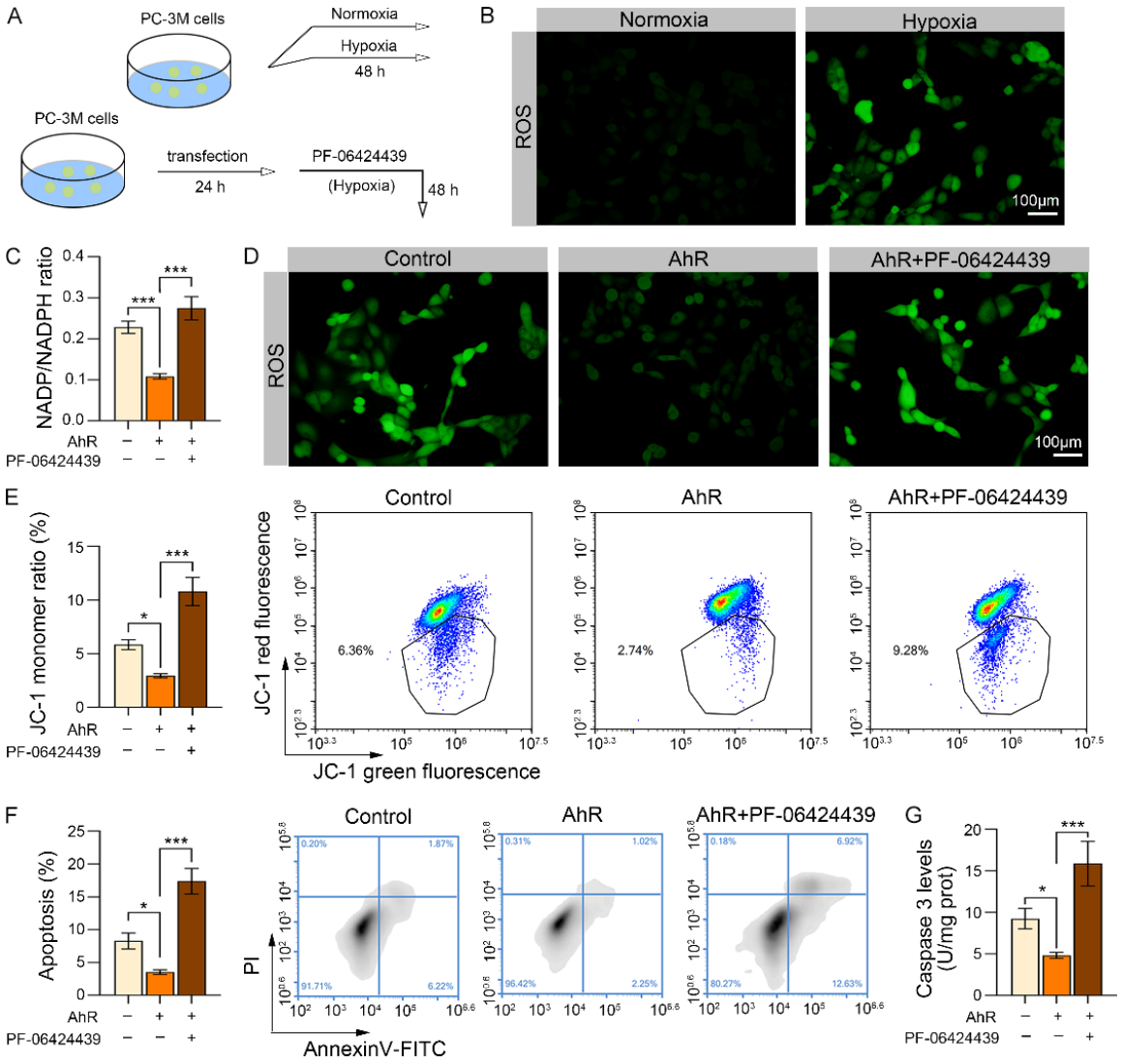

Figure 2. AhR-dependent LD generation promotes oxidative stress adaptation in PC-3M cells and alleviates mitochondrial dysfunction. (A, B) After incubation under normoxic or hypoxic conditions for 48 h, intracellular ROS were measured using the DCFH-DA fluorescent probe (B). Scale bar, 100 μm, 200×. At 24 h post-transfection, PC-3M cells were treated with 10 μM PF-06424439 under hypoxic conditions for 48 h, followed by downstream experimental use. (C) $NADP^+$/NADPH ratio analysis in PC-3M cells. One-way ANOVA, ***$P < 0.001$, AhR vs. Control, AhR+PF-06424439 vs. AhR. $n = 3$. (D) DCFH-DA-based analysis of ROS levels in PC-3M cells. $n = 3$. Scale bar, 100 μm, 200×. (E) Treated-PC-3M cells were stained with the JC-1 probe and then analyzed by flow cytometry. One-way ANOVA, *$P < 0.05$, AhR vs. Control; ***$P < 0.001$, AhR+PF-06424439 vs. AhR. $n = 3$. (F) Flow cytometry-based analysis of PC-3M cell apoptosis with corresponding quantification. One-way ANOVA, *$P < 0.05$, AhR vs. Control; ***$P < 0.001$, AhR+PF-06424439 vs. AhR. $n = 3$. (G) Caspase 3 levels in PC-3M cells. One-way ANOVA, *$P < 0.05$, AhR vs. Control; ***$P < 0.001$, AhR+PF-06424439 vs. AhR. $n = 3$.

following AhR overexpression in hypoxia-induced PC-3M cells (**Figure 3A**), while they were reduced after AhR knockdown (**Figure 3B**). LD formation after AhR overexpression was inhibited by LY294002 (a PI3K inhibitor) in hypoxia-induced PC-3M cells (**Figure 3C**), and the expression of active caspase-3 was also increased upon inhibitor treatment (**Figure 3D**). These results demonstrate that AhR promotes LD formation via the PI3K/AKT pathway, thereby suppressing the apoptotic death of hypoxia-induced PC-3M cells.

AhR activates the PI3K/AKT pathway through RAB3D

AhR has previously been shown to upregulate RAB3D, which in turn promotes PCa progres-

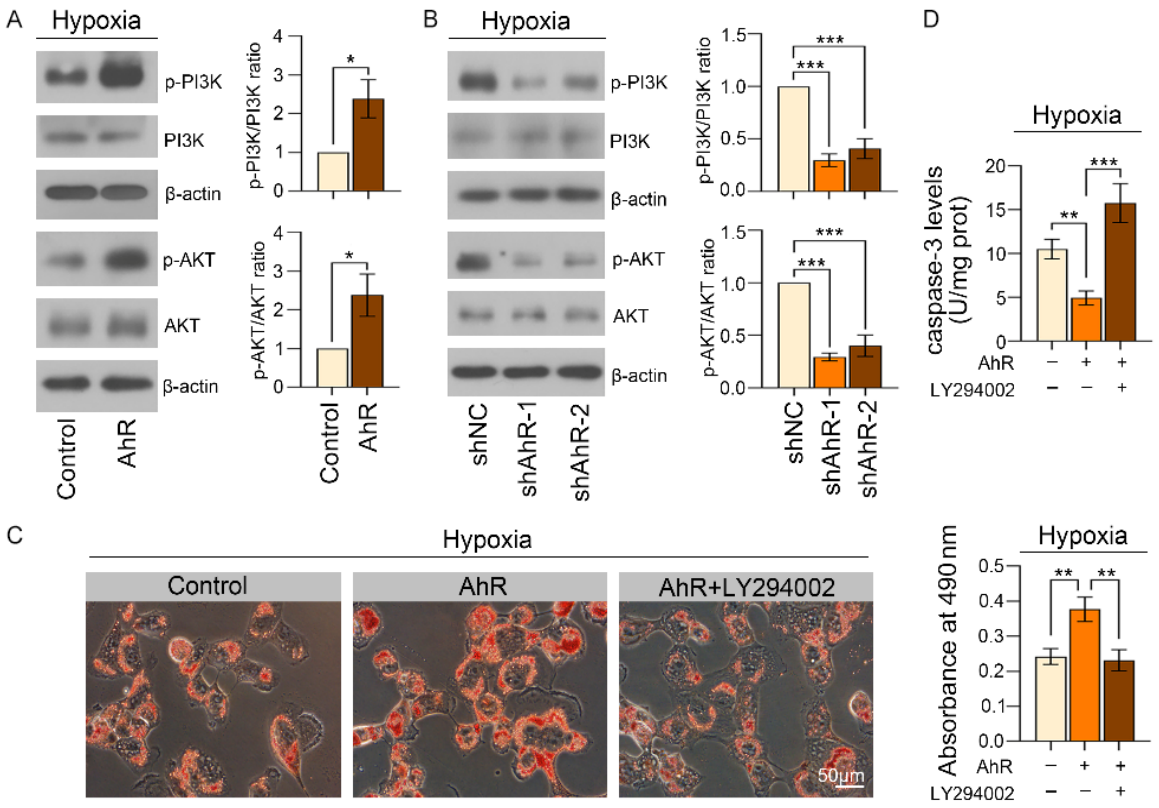

Figure 3. AhR promotes LD formation via PI3K/AKT pathway activation. (A, B) p-PI3K and p-AKT protein levels in PC-3M cells after AhR overexpression (A) or knockdown (B). Student's t-test, **P* < 0.05, AhR vs. Control; One-way ANOVA, ****P* < 0.001, shAhR-1 or shAhR-2 vs. shNC. *n* = 3. (C) LD formation was measured after AhR overexpression and LY294002 treatment. Scale bar, 50 μm, 400×. One-way ANOVA, ***P* < 0.01, AhR vs. Control; ***P* < 0.01, AhR+LY294002 vs. AhR. *n* = 3. (D) Caspase 3 content in PC-3M cells. One-way ANOVA, ***P* < 0.01, AhR vs. Control; ****P* < 0.001, AhR+LY294002 vs. AhR. *n* = 3.

sion by activating the PI3K/AKT pathway [19]. In the present study, we sought to investigate whether RAB3D was involved in the activation of the PI3K/AKT pathway by AhR in hypoxia-induced PC-3M cells. We successfully knocked down RAB3D in PC-3M cells (**Figure 4A**, **4B**). In hypoxia-induced PC-3M cells, AhR overexpression promoted the expression of RAB3D, and this process was reversed by RAB3D knockdown (**Figure 4C**). As expected, in hypoxia-induced PC-3M cells, the overexpression of AhR increased the levels of p-PI3K and p-AKT (**Figure 4D**), whereas RAB3D knockdown inhibited the expression of p-PI3K and p-AKT (**Figure 4E**). These findings indicated that under hypoxic conditions, AhR still activated the PI3K/AKT pathway through RAB3D. Additionally, RAB3D knockdown inhibited the formation of LDs in hypoxia-induced PC-3M cells (**Figure 4F**). Knocking down RAB3D increased apoptosis in PC-3M cells, as evidenced by elevated levels of cleaved caspase-3 (**Figure 4G**). Therefore, AhR promotes LD formation and inhibits cellular apoptosis through a mechanism at least partially mediated by RAB3D.

CYLD blocks the K63 ubiquitination of AhR, thereby reducing its activity

Lastly, the mechanisms governing AhR regulation were analyzed at length. CYLD is a deubiquitinating enzyme that removes K63-linked ubiquitin chains [16]. Online database analyses suggested a potential binding interaction between CYLD and AhR [20]. To test the ability of CYLD to mediate deubiquitination of AhR, we therefore constructed a CYLD overexpression vector and successfully overexpressed CYLD in PC-3M cells (**Figure 5A**). Under hypoxic conditions, CYLD overexpression inhibited the nuclear expression of AhR, suggesting that CYLD suppressed AhR activation (**Figure 5B**). Co-IP assays verified the interaction between CYLD

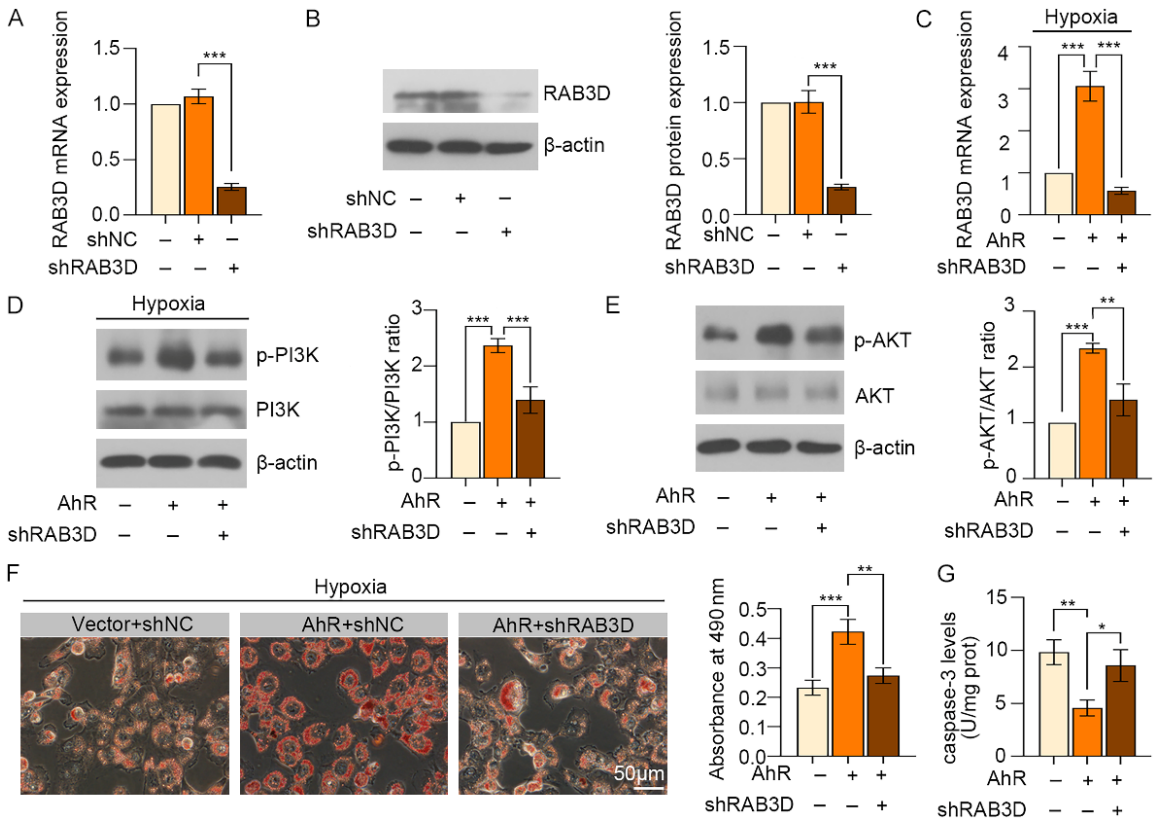

Figure 4. AhR activates the PI3K/AKT pathway through RAB3D. (A, B) RAB3D was knocked down in PC-3M cells, and the expression of AhR was analyzed by Real-time PCR (A) and Western blotting (B). One-way ANOVA, ***P < 0.001, shRAB3D vs. shNC. n = 3. (C) RAB3D was knocked down in AhR-overexpressing PC-3M cells, and the expression of AhR and RAB3D at the mRNA level was measured. One-way ANOVA, ***P < 0.001, AhR vs. Control, shRAB3D vs. shNC. n = 3. (D, E) Analyses of p-PI3K (D) and p-AKT (E) protein levels in PC-3M cells after AhR was overexpressed and RAB3D was knocked down. One-way ANOVA, **P < 0.01, ***P < 0.001, AhR vs. Control, shRAB3D vs. shNC. n = 3. (F) Measurement of LD formation after AhR overexpression and RAB3D knockdown. Scale bar, 50 μm, 400×. One-way ANOVA, ***P < 0.001, AhR vs. Control; **P < 0.01, shRAB3D vs. shNC. n = 3. (G) Caspase 3 content in PC-3M cells. One-way ANOVA, **P < 0.01, AhR vs. Control; *P < 0.05, shRAB3D vs. shNC. n = 3.

and AhR (**Figure 5C**), and CYLD reduced the extent of the K63-linked ubiquitination of AhR (**Figure 5D**). CYLD overexpression also suppressed LD formation (**Figure 5E**) and increased active caspase-3 levels in hypoxia-induced PC-3M cells (**Figure 5F**). Collectively, these results indicated that CYLD inhibits the activation of AhR by removing its K63-linked ubiquitination (**Figure 5G**), thereby inhibiting LD formation and promoting apoptotic cell death.

Discussion

In this study, we report a novel role for hypoxia-induced LD accumulation in the AhR-mediated promotion of PCa progression. We found that, under hypoxic conditions, LD storage was crucial for AhR to alleviate oxidative damage and mitochondrial dysfunction in PC-3M cells. This may represent a mechanism by which PCa cells maintain their cancerous properties even in the absence of hormonal stimulation.

Hypoxia is a common characteristic of solid tumors, leading to numerous transcriptional and post-translational changes that sustain tumor survival [21, 22], with these changes playing a particularly important role in PCa [23]. Tumor microenvironmental factors such as hypoxia stimulate cancer cells to produce large amounts of ROS [24]. However, prolonged exposure to high levels of ROS may induce oxidative stress, exacerbating tumor cell damage [25]. LDs play a crucial role in the intratumoral oxidative stress response. They promote tumorigenesis through the storage, transport, and distribution of fatty acids and lipids [26]. By buffering oxidative stress, LDs facilitate cellular redox

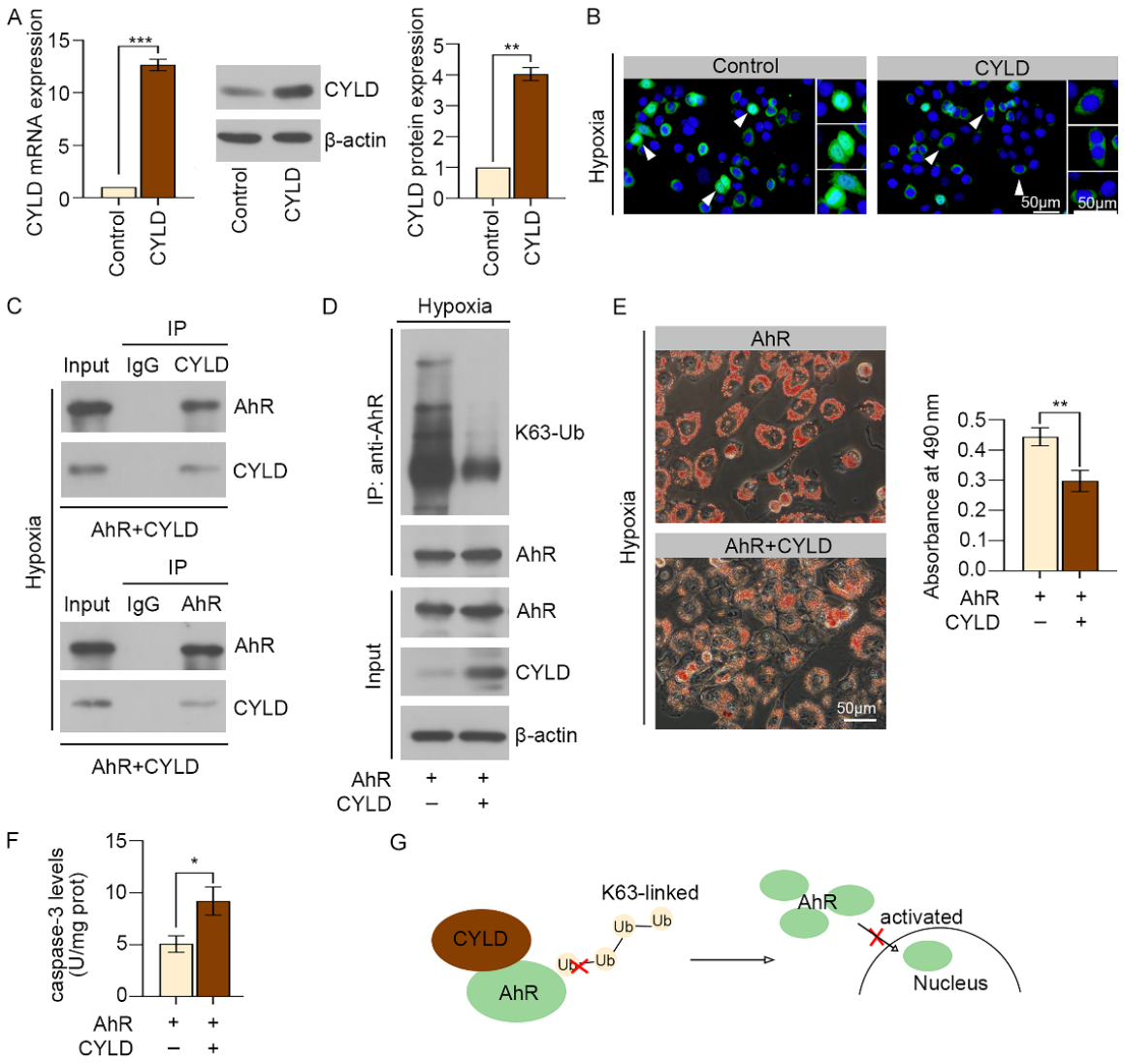

Figure 5. CYLD reduces AhR activity by blocking its K63 ubiquitination. A. Confirmation of CYLD overexpression in PC-3M cells at the mRNA and protein levels. Student's t-test, $^{**}P < 0.01$, $^{***}P < 0.001$, CYLD vs. Control. B. The distribution of AhR in CYLD overexpressed-PC-3M cells as detected by immunofluorescence. Scale bar, 50 μm, 400×. C. Co-IP analysis of the interaction between AhR and CYLD. D. Analysis of AhR K63-linked ubiquitination levels in CYLD-overexpressing PC-3M cells. E. Analysis of LD formation after CYLD overexpression. Scale bar, 50 μm, 400×. Student's t-test, $^{**}P < 0.01$, AhR+CYLD vs. AhR. F. Caspase 3 content in PC-3M cells after CYLD overexpression. Student's t-test, $^{*}P < 0.05$, AhR+CYLD vs. AhR. G. CYLD inhibited the activation of AhR by suppressing the K63-linked ubiquitination of AhR. Student's t-test, $^{**}P < 0.01$, AhR vs. Control.

homeostasis, which is essential for the survival, growth, and proliferation of cancer cells [26]. Studies have shown that hypoxic environments induce LD accumulation in tumor cells [27], consistent with the present results. We further found that the hypoxia-induced LD accumulation in PC-3M cells is dependent on the expression of AhR. Ohashi et al. previously demonstrated that AhR promotes hepatic LD accumulation [13], while Wang et al. reported that AhR enhances LD biogenesis in bronchiolar exocrine cells [14]. However, the mechanism by which AhR induces LD accumulation in PC-3M cells under hypoxic conditions has not previously been clarified. Activation of the PI3K/AKT pathway has also been shown to promote intracellular LD accumulation [28]. Research by Xie et al. revealed the activation of the PI3K/AKT pathway under hypoxic conditions [29], in line with our findings. We therefore hypothesized that AhR may promote LD formation by activating the PI3K/AKT pathway.

Consistently, we found that treatment with LY294002 inhibited AhR-induced LD accumulation under hypoxic conditions, confirming that AhR can promote LDs formation by activating the PI3K/AKT pathway in a hypoxic environment. In a previous study, we demonstrated that RAB3D is upregulated by AhR and promotes the progression of PCa by activating the PI3K/AKT pathway [19]. Here, we further confirmed that this process also takes place in PC-3M cells under hypoxic treatment conditions. In summary, we found that in hypoxia-induced PC-3M cells, AhR triggers RAB3D upregulation, in turn promoting the activation of the PI3K/AKT pathway and facilitating LD formation.

Under hypoxic conditions, mitochondrial ROS levels are significantly elevated, exacerbating cellular oxidative damage and mitochondrial dysfunction [25]. Abreu et al. demonstrated that hypoxia induces a substantial increase in ROS levels in tumor cells [30], and these ROS can further aggravate mitochondrial damage in tumor cells [31], consistent with the phenomena observed in our study. However, we found that AhR overexpression effectively alleviated hypoxia-induced damage, as evidenced by reduced ROS levels and a decreased NADH/NADPH ratio. Moreover, AhR overexpression restored mitochondrial membrane potential and reduced apoptotic cell death. LDs have been reported to protect glioma and breast cancer cells from ROS-associated toxicity under hypoxic conditions [32]. The formation of LDs in gastric cancer cells also reportedly mitigates the occurrence of oxidative stress [33], and Oyer et al. found that LDs can sequester toxic levels of ROS in PCa cells, preserving redox homeostasis and sustaining proliferation [34]. In line with these findings, we noted that AhR overexpression alleviated hypoxia-induced oxidative damage and mitochondrial dysfunction in PC-3M cells, while this effect was abrogated following treatment with an LD inhibitor. LDs can form lipid droplet-mitochondria contact sites, thereby trapping excess ROS produced by mitochondria and preventing their diffusion into the cytoplasm to induce oxidative damage [35]. Additionally, intermediate products of LD metabolism generate NADPH through enzyme-catalyzed processes, providing reducing power for the synthesis of antioxidant molecules and enhancing cellular capacity for ROS scavenging [33]. These factors may collectively explain how AhR promotes LD formation to alleviate oxidative damage and mitochondrial dysfunction in PC-3M cells under hypoxic conditions.

The mechanisms governing AhR regulation were also explored at length. While prior reports have documented several regulatory processes, the K63 ubiquitination of AhR has been established as an activating modification [17]. CYLD is a deubiquitinating enzyme that specifically removes K63-linked ubiquitin chains [36], and CYLD deficiency has been reported to promote the proliferation and survival of PCa cells, as well as tumor growth [18]. This raised the possibility that CYLD may affect the progression of PCa by regulating the extent of AhR K63 ubiquitination. Consistent with this hypothesis, we observed an interaction between CYLD and AhR, and found that CYLD inhibited both the level of K63 ubiquitination of AhR as well as the nuclear translocation of AhR. This confirmed the ability of CYLD to suppress AhR activity.

In summary, we specifically determined that AhR protects PCa cells from the toxic damage caused by ROS under hypoxic conditions by promoting the formation of LDs.

Acknowledgements

This study was supported by the High-level Talents Introduction Scientific Research Start-up Fund of Liuzhou People's Hospital (LRYGCC202304), the National Natural Science Foundation of China (82360491) and Liuzhou Science and Technology Plan Project (2024YB0101A007).

Disclosure of conflict of interest

None.

Address correspondence to: Jingsong Yu, Department of Urology, Liuzhou People's Hospital Affiliated to Guangxi Medical University, No. 8 Wenchang Road, Liuzhou 545006, Guangxi, The People's Republic of China. E-mail: qt000330@sr.gxmu.edu.cn

References

[1] Almeeri MNE, Awies M and Constantinou C. Prostate cancer, pathophysiology and recent developments in management: a narrative review. Curr Oncol Rep 2024; 26: 1511-1519.

[2] Sternberg CN and Morgans AK. Treatment options in hormone-sensitive prostate cancer: targeting the androgen-sensitive pathway. Future Oncol 2025; 21: 3227-3235.
[3] Zhang Y, Wang P, Jia Z, Zheng Z, Wang J and Liang H. Global burden and risk factors of male cancers from 1990 to 2021, with forecasts to 2040. Sci Rep 2025; 15: 5123.
[4] Chukhu M, Dahiya UR and Heemers HV. Evolving roles for the androgen receptor and its protein interactome in castration-resistant prostate cancer. Oncogene 2025; 44: 3883-3894.
[5] Kim WK, Buckley AJ, Lee DH, Hiroto A, Nenninger CH, Olson AW, Wang J, Li Z, Vikram R, Adzavon YM, Yau TY, Bao Y, Kahn M, Geradts J, Xiao GQ and Sun Z. Androgen deprivation induces double-null prostate cancer via aberrant nuclear export and ribosomal biogenesis through HGF and Wnt activation. Nat Commun 2024; 15: 1231.
[6] Mendoza EN, Ciriolo MR and Ciccarone F. Hypoxia-induced reactive oxygen species: their role in cancer resistance and emerging therapies to overcome it. Antioxidants (Basel) 2025; 14: 94.
[7] Chen D, Guo Z, Yao L, Sun Y, Dian Y, Zhao D, Ke Y, Zeng F, Zhang C, Deng G and Li L. Targeting oxidative stress-mediated regulated cell death as a vulnerability in cancer. Redox Biol 2025; 84: 103686.
[8] Zhang R, Meng J, Yang S, Liu W, Shi L, Zeng J, Chang J, Liang B, Liu N and Xing D. Recent advances on the role of ATGL in cancer. Front Oncol 2022; 12: 944025.
[9] Petan T, Jarc E and Jusović M. Lipid droplets in cancer: guardians of fat in a stressful world. Molecules 2018; 23: 1941.
[10] Schulte KW, Green E, Wilz A, Platten M and Daumke O. Structural basis for aryl hydrocarbon receptor-mediated gene activation. Structure 2017; 25: 1025-1033, e1023.
[11] Xue P, Fu J and Zhou Y. The aryl hydrocarbon receptor and tumor immunity. Front Immunol 2018; 9: 286.
[12] Richmond O, Ghotbaddini M, Allen C, Walker A, Zahir S and Powell JB. The aryl hydrocarbon receptor is constitutively active in advanced prostate cancer cells. PLoS One 2014; 9: e95058.
[13] Ohashi H, Nishioka K, Nakajima S, Kim S, Suzuki R, Aizaki H, Fukasawa M, Kamisuki S, Sugawara F, Ohtani N, Muramatsu M, Wakita T and Watashi K. The aryl hydrocarbon receptor-cytochrome P450 1A1 pathway controls lipid accumulation and enhances the permissiveness for hepatitis C virus assembly. J Biol Chem 2018; 293: 19559-19571.
[14] Wang HC, Liu KY, Wang LT, Hsu SH, Wang SC and Huang SK. Aryl hydrocarbon receptor promotes lipid droplet biogenesis and metabolic shift in respiratory club cells. Hum Cell 2021; 34: 785-799.
[15] Fontaine A, Bellanger D, Guibon R, Bruyère F, Brisson L and Fromont G. Lipophagy and prostate cancer: association with disease aggressiveness and proximity to periprostatic adipose tissue. J Pathol 2021; 255: 166-176.
[16] Zhu G, Herlyn M and Yang X. TRIM15 and CYLD regulate ERK activation via lysine-63-linked polyubiquitination. Nat Cell Biol 2021; 23: 978-991.
[17] Wang W, Xiang T, Yang Y, Wang Z and Xie J. E3 ubiquitin ligases STUB1/CHIP contributes to the Th17/Treg imbalance via the ubiquitination of aryl hydrocarbon receptor in rheumatoid arthritis. Clin Exp Immunol 2022; 209: 280-290.
[18] Yang WL, Jin G, Li CF, Jeong YS, Moten A, Xu D, Feng Z, Chen W, Cai Z, Darnay B, Gu W and Lin HK. Cycles of ubiquitination and deubiquitination critically regulate growth factor-mediated activation of Akt signaling. Sci Signal 2013; 6: ra3.
[19] Yu J, Qi H, Wang Z, Zhang Z, Song E, Song W and An R. RAB3D, upregulated by aryl hydrocarbon receptor (AhR), promotes the progression of prostate cancer by activating the PI3K/AKT signaling pathway. Cell Biol Int 2022; 46: 2246-2256.
[20] Garcia-Garcia J, Valls-Comamala V, Guney E, Andreu D, Muñoz FJ, Fernandez-Fuentes N and Oliva B. iFrag: a protein-protein interface prediction server based on sequence fragments. J Mol Biol 2017; 429: 382-389.
[21] Semenza GL. Hypoxia-inducible factor 1 (HIF-1) pathway. Sci STKE 2007; 2007: cm8.
[22] Selfridge AC, Cavadas MA, Scholz CC, Campbell EL, Welch LC, Lecuona E, Colgan SP, Barrett KE, Sporn PH, Sznajder JI, Cummins EP and Taylor CT. Hypercapnia suppresses the HIF-dependent adaptive response to hypoxia. J Biol Chem 2016; 291: 11800-11808.
[23] Zhong J, Frood R, McWilliam A, Davey A, Shortall J, Swinton M, Hulson O, West CM, Buckley D, Brown S, Choudhury A, Hoskin P, Henry A and Scarsbrook A. Prediction of prostate tumour hypoxia using pre-treatment MRI-derived radiomics: preliminary findings. Radiol Med 2023; 128: 765-774.
[24] Hacker L, Sarsam E, Conway SJ and Hammond EM. A guide to reactive oxygen species in tumour hypoxia: measurement and therapeutic implications. Mol Oncol 2025; 19: 3003-3022.
[25] Cairns RA, Harris IS and Mak TW. Regulation of cancer cell metabolism. Nat Rev Cancer 2011; 11: 85-95.
[26] Kawaguchi K, Kinameri A, Suzuki S, Senga S, Ke Y and Fujii H. The cancer-promoting gene

fatty acid-binding protein 5 (FABP5) is epigenetically regulated during human prostate carcinogenesis. Biochem J 2016; 473: 449-461.
[27] Chauhan SS, Vizzerra AD, Liou H, Flores CE, Snider AJ, Snider JM and Warfel NA. Hypoxia induced lipid droplet accumulation promotes resistance to ferroptosis in prostate cancer. Oncotarget 2025; 16: 532-544.
[28] Yue S, Li J, Lee SY, Lee HJ, Shao T, Song B, Cheng L, Masterson TA, Liu X, Ratliff TL and Cheng JX. Cholesteryl ester accumulation induced by PTEN loss and PI3K/AKT activation underlies human prostate cancer aggressiveness. Cell Metab 2014; 19: 393-406.
[29] Xie Y, Qi Y, Zhang Y, Chen J, Wu T and Gu Y. Regulation of angiogenic factors by the PI3K/Akt pathway in A549 lung cancer cells under hypoxic conditions. Oncol Lett 2017; 13: 2909-2914.
[30] Lacerda-Abreu MA, Carvalho-Kelly LF and Meyer-Fernandes JR. Hypoxia modulates transmembrane prostatic acid phosphatase (TM-PAP) in MCF-7 breast cancer cells. Int J Mol Sci 2025; 26: 1918.
[31] Weinberg F, Ramnath N and Nagrath D. Reactive oxygen species in the tumor microenvironment: an overview. Cancers (Basel) 2019; 11: 1191.
[32] Bensaad K, Favaro E, Lewis CA, Peck B, Lord S, Collins JM, Pinnick KE, Wigfield S, Buffa FM, Li JL, Zhang Q, Wakelam MJO, Karpe F, Schulze A and Harris AL. Fatty acid uptake and lipid storage induced by HIF-1α contribute to cell growth and survival after hypoxia-reoxygenation. Cell Rep 2014; 9: 349-365.
[33] Li S, Wu T, Lu YX, Wang JX, Yu FH, Yang MZ, Huang YJ, Li ZJ, Wang SL, Huang L, Lu L and Tian T. Obesity promotes gastric cancer metastasis via diacylglycerol acyltransferase 2-dependent lipid droplets accumulation and redox homeostasis. Redox Biol 2020; 36: 101596.
[34] Oyer HM, Steck AR, Longen CG, Venkat S, Bayrak K, Munger EB, Fu D, Castagnino PA, Sanders CM, Tancler NA, Mai MT, Myers JP, Schiewer MJ, Chen N, Mostaghel EA and Kim FJ. Sigma1 regulates lipid droplet-mediated redox homeostasis required for prostate cancer proliferation. Cancer Res Commun 2023; 3: 2195-2210.
[35] Fan H and Tan Y. Lipid droplet-mitochondria contacts in health and disease. Int J Mol Sci 2024; 25: 6878.
[36] Blake PW and Toro JR. Update of cylindromatosis gene (CYLD) mutations in Brooke-Spiegler syndrome: novel insights into the role of deubiquitination in cell signaling. Hum Mutat 2009; 30: 1025-1036.

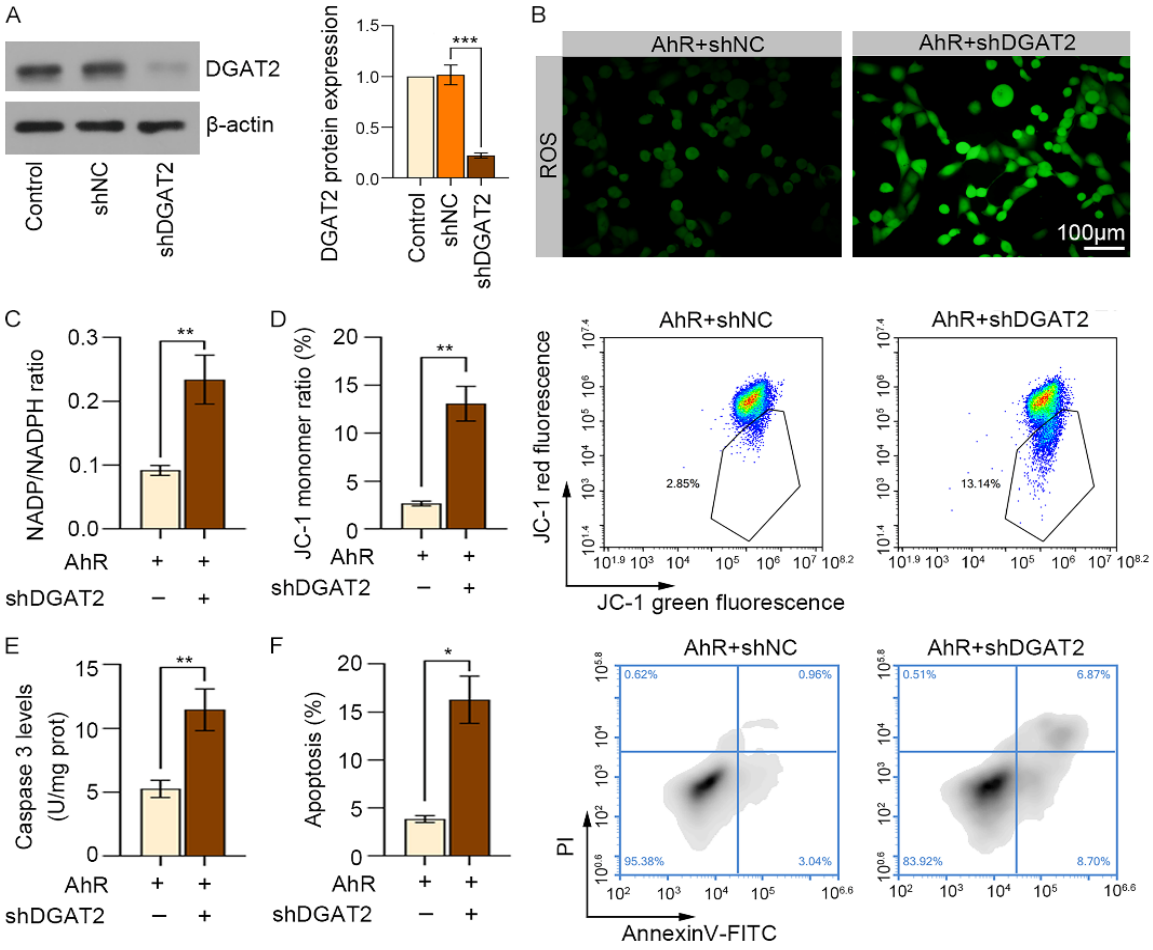

Supplementary Figure 1. PI3K/AKT pathway activation is evident in hypoxia-induced PC-3M cells. A. DGAT2 was knocked down in PC-3M cells. One-way ANOVA, ***P < 0.001, shDGAT2 vs. shNC. B. ROS levels were detected with DCFH-DA in PC-3M cells. n = 3. Scale bar, 100 μm, magnification 200×. C. $NADP^+$/NADPH ratio in PC-3M cells. Student's t-test, **P < 0.01, shDGAT2 vs. shNC. n = 3. D. PC-3M cells were stained with the JC-1 probe and then analyzed by flow cytometry. Student's t-test, **P < 0.01, shDGAT2 vs. shNC. n = 3. E. Caspase 3 content in PC-3M cells. Student's t-test, **P < 0.01, shDGAT2 vs. shNC. n = 3. F. Apoptosis in PC-3M cells was analyzed by flow cytometry with corresponding quantification. Student's t-test, *P < 0.05, shDGAT2 vs. shNC. n = 3.

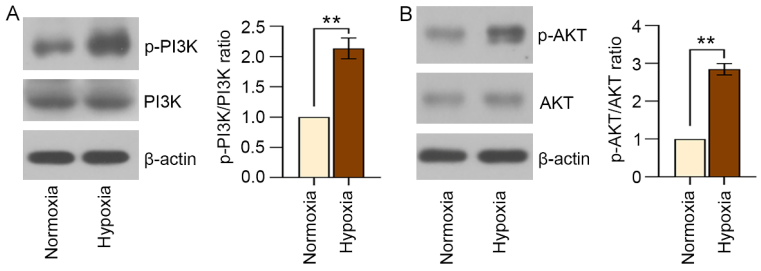

Supplementary Figure 2. The PI3K/AKT pathway was activated in hypoxia-induced PC-3M cells. (A, B) PC-3M cells were exposed to hypoxia for 48 h, and the cells were then lysed for western blotting. Phosphorylated forms of PI3K (p-PI3K) (A) and AKT (p-AKT) (B) were detected and normalized to total PI3K and AKT. Student's t-test, **P < 0.01, Hypoxia vs. Normoxia. n = 3.